Available online at www.sciencedirect.com
SCIENCE DIRECT
Journal of Molecular Catalysis A: Chemical 253 (2006) 270–278
JOURNAL OF MOLECULAR CATALYSIS A: CHEMICAL
www.elsevier.com/locate/molcata

Cu/Zn-based catalysts improved by adding magnesium for water–gas shift reaction

Tetsuya Shishido [a], Manabu Yamamoto [b], Ikuo Atake [b], Dalin Li [b], Yan Tian [a], Hiroyuki Morioka [c], Masahide Honda [c], Tsuneji Sano [b], Katsuomi Takehira [b,*]

[a] *Department of Chemistry, Tokyo Gakugei University, Nukui-Kita 4-1-1, Koganei, Tokyo 184-8501, Japan*
[b] *Department of Chemistry and Chemical Engineering, Graduate School of Engineering, Hiroshima University, Kagamiyama 1-4-1, Higashi-Hiroshima 739-8527, Japan*
[c] *Hiroshima Prefectural Institute of Industrial Science and Technology, Kagamiyama 3-10-32, Higashi-Hiroshima 739-0046, Japan*

Received 9 November 2005; received in revised form 16 March 2006; accepted 22 March 2006
Available online 27 April 2006

Abstract

Ternary Cu/MeO/ZnO (Me: alkaline-earth metal, Mg, Ca, Sr and Ba) catalysts were prepared by homogeneous precipitation (hp) using urea hydrolysis. The structure and the activity for the water–gas shift reaction of these catalysts were studied compared with those of the catalysts prepared by coprecipitation (cp). The highest activity was obtained over hp-Cu/MgO/ZnO among the catalysts tested. The catalyst precursors after the precipitation contained mainly aurichalcite, $(Cu,Zn)_5(CO_3)_2(OH)_{16}$, while the decomposed products after the calcination contained apparently CuO and ZnO as crystalline phases, since the amount of Mg actually included in the catalyst was less than 1.0 at.%. The Cu metal surface area was larger and the particle size of Cu metal was smaller on the hp-catalysts than those on the cp-catalysts; nonetheless the BET surface area was sometimes larger on the latter than on the former. The addition of ∼0.1 at.% of Mg was the most effective, resulting in the highest activity as well as the lowest activation energy. A good correlation was observed between the amount of Cu^+ species and the activation energy of the shift reaction, suggesting that MgO significantly enhanced the formation of Cu^+ species as the active sites. Even after the pre-reduction at the high temperature, 250 °C, hp-Cu/MgO/ZnO catalyst showed no significant decrease in the activity as well as no detectable sintering in the Cu metal particles during 50 h of the reaction. It was supposed that the shift reaction proceeds by a reduction–oxidation mechanism between $Cu^0 \leftrightarrow Cu^+$.

Keywords: Hydrogen production; Water–gas shift reaction; Cu/MgO/ZnO catalyst; Cu^+ species; Homogeneous precipitation

1. Introduction

The most widely employed way to produce hydrogen is the steam reforming of hydrocarbons and is of importance for future energy technologies such as fuel cells. Hydrogen has been used as a fuel for polymer electrolyte fuel cells (PEFCs), and the Pt electrode on PEFC is not tolerant to fuels containing CO more than 20 ppm. It is necessary to achieve low levels of CO by removal from reformed gas. CO is a coproduct of the reforming reaction and most of the CO produced is converted to hydrogen by the water–gas shift reaction [1–19]. The shift reaction is desirable for removal of a large amount of CO since it is moderately exothermic reaction ($\Delta H_{298} = -41.1$ kJ mol^{-1}) and the reaction temperature is easy to control. The equilibrium conversion of CO is dependent largely on the reaction temperature; lower temperature is favored for higher CO removal. On the other hand, from the viewpoint of kinetics, the reactant gases are not active enough to reach the chemical equilibrium at low temperature. Copper-based catalysts are generally more active for the shift reaction, but are more unstable to oxidant gases than precious metal catalysts. It is, therefore, important to develop highly stable Cu-based catalysts [10–19] or highly active precious metal catalysts [1–9]. As for the recent work over the precious metal catalysts, Au/Fe_2O_3 [1,4], Au/TiO_2 [1,5], Au/CeO_2 [8], Pt/CeO_2 [2–4], Pt/TiO_2 [9], Ru/Fe_2O_3 [6] and Pd, Pt and Rh/Fe_2O_3 [7] have been prepared by various methods and studied for the shift reaction.

Ternary $Cu/ZnO/Al_2O_3$ catalysts have been widely employed commercially since the early 1960s in the water–gas shift reaction; the catalyst was usually prepared by coprecipitation to

* Corresponding author. Tel.: +81 82 424 7744; fax: +81 82 424 7744.
E-mail address: takehira@hiroshima-u.ac.jp (K. Takehira).

1381-1169/$ – see front matter © 2006 Elsevier B.V. All rights reserved.
doi:10.1016/j.molcata.2006.03.049

afford the higher Cu metal dispersion in the resulting catalyst and, as a consequence, the higher catalytic activity [10]. Coprecipitated Cu/ZnO/Al_2O_3 catalysts were more sustainable than the impregnated catalysts in the shift reaction [14]. The application of hydrogen production to PEFCs involves frequent start-ups and shut-downs. The catalysts for the shift reaction are, therefore, sometimes exposed to water and/or oxygen containing atmosphere at low temperatures. To improve the stability of Cu/ZnO catalyst, CeO_2 impregnation [19], spinel formation of Cu–Al–Zn oxides [11] or $CuMn_2O_4$ [16–18] have been proposed. When the spinel oxides were calcined above 900 °C, Cu^{2+} was easily reduced and this may be responsible for the high activity of the spinel compounds [16]. Partial substitution of Fe or Al for Mn enhanced the catalytic activity and, moreover, urea homogeneous coprecipitation method and sol–gel method, such as citric acid complex method, were effective for the preparation of active Cu–Mn spinel catalyst [18].

We have studied on the preparation method of highly active supported Ni catalysts for steam, dry or autothermal reforming of CH_4 by the citrate method [20,21] and coprecipitation method [22–24]. Recently, we have reported that Cu/ZnO and Cu/ZnO/Al_2O_3 catalysts were prepared by homogeneous precipitation (hp) using urea hydrolysis and were successfully applied to hydrogen production by steam reforming of methanol [25] and the CO shift reaction [26]. The hp-catalysts showed higher activities than those prepared by coprecipitation (cp). It was suggested that the good catalytic performance of hp-Cu/ZnO are due to both highly dispersed Cu metal species and, as a result, to high accessibility of the Cu metal species to methanol, CO and steam. It was concluded that the homogeneous precipitation method by urea hydrolysis is favorable for the preparation of active Cu/ZnO catalysts. In the present work, we report the high and stable activity of Cu/MgO/ZnO catalysts prepared by the urea homogeneous precipitation method in the shift reaction.

2. Experimental

2.1. Preparation of the catalysts

Cu/MgO/ZnO catalysts were prepared by two methods, i.e. coprecipitation (cp) and homogeneous precipitation (hp) by urea hydrolysis. In the cp-method, the aqueous solution of metal nitrates was dropped into aqueous solution of Na_2CO_3 with vigorous stirring and the pH was adjusted at 7 with NaOH. The obtained precipitate was dried at 80 °C, followed by calcination at 300 °C for 3 h in air. The hp-method was achieved by urea hydrolysis [27–29] as follows: calculated amounts of metal nitrates and urea were dissolved in deionized water at room temperature and heated at 90 °C for 24 h to hydrolyze urea. During the hydrolysis of urea, hydroxide ions are generated in the homogeneous solution (Eq. (1)), which hydrolyzed metal nitrates to the corresponding

$$CO(NH_2)_2 + H_2O \rightarrow 2NH_4^+ + HCO_3^- + OH^- \quad (1)$$

hydroxides to finally form the hydroxycarbonates (vide infra) as the catalyst precursors. After the heating, the mixture was cooled at 0 °C for 0.5 h, and the precipitates were filtrated by a glass filter and washed with 1 l of deionized water. The precipitates were dried at 100 °C for 12 h, followed by calcination at 300 °C for 3 h in air. It is expected that the homogeneity of the precipitate obtained by this method will be higher than that prepared by conventional coprecipitation, since there is no gradient in concentration of precipitants in the solution. The other ternary Cu/MeO/ZnO (Me: Ca, Sr and Ba) catalysts ere also prepared by the hp-method.

Moreover, several Cu/MgO/ZnO catalysts were prepared by changing the metal contents which are shown in the parentheses after the catalyst symbol, e.g. Cu/MgO/ZnO (45/5/50). The number in parentheses shows the metal composition calculated from the amount of raw materials in the catalyst preparation. The analytical results of metal content by ICP showed that both Cu and Zn were quantitatively incorporated in the catalysts but Mg was not efficiently incorporated in the catalyst probably due to pH value at 7.0 in the catalyst preparation (vide infra).

2.2. Characterization of the catalysts

The structure of the catalysts was studied by using XRD, EXAFS, XPS, AES, STEM, ICP, N_2O decomposition and N_2 adsorption method.

Powder X-ray diffraction was recorded on a Rigaku powder diffraction unit, RINT 2250VHF, with mono-chromatized Cu Kα radiation ($\lambda = 0.154$ nm) at 40 kV and 300 mA. The diffraction pattern was identified by comparing with those included in the JCPDS (Joint Committee of Powder Diffraction Standards) database.

X-ray absorption spectroscopic measurements were performed with synchrotron radiation at a beam line BL7C station of the photon factory, at the High Energy Accelerator Research Organization (Tsukuba, Japan), operated at 2.5 GeV with about 35–380 mA of ring current. The data were recorded in transmission mode at room temperature using Si (1 1 1) double crystal monochrometer. Energy was calibrated with Cu K-edge absorption (8981.0 eV), and the energy step of measurement in the XANES region was 0.3 eV. The data analysis was performed using the REX2000 Ver. 2.3 (Rigaku). For the extended X-ray absorption fine structure (EXAFS) analysis, the oscillation was extracted from the EXAFS data by a spline smoothing method [30]. The oscillation was normalized by edge height around 50 eV higher than the absorption edge.

X-ray photoelectron spectroscopy (XPS) and Auger electron spectroscopy (AES) were performed with a VG Scientific ESCALAB220i-XL spectrometer by using monochromatic Al Kα and Au mesh as the sample holder. Before measuring the spectra, samples were pre-reduced at 300 °C for 1 h under the mixed gas flow of H_2/N_2 (1/19 ml min^{-1}).

Scanning transmission electron microscope (STEM) measurements were performed with a JEOL JEM-3000F microscope by using a Noran Voyager energy dispersive X-ray spectroscopy at an accelerating voltage of 300 kV.

Inductively coupled plasma (ICP) optical emission spectrometry was used for the determination of the metal content in each sample synthesized above. The measurements were performed

with a Perkin-Elmer OPTIMA 3000 apparatus, and the sample was dissolved in a mixture of HF and HNO_3 acids before the measurements.

The copper metal surface areas were determined by N_2O decomposition method at 90 °C as reported by Evans et al. [31], assuming a reaction stoichiometry of two Cu atoms per oxygen atom and a Cu surface density of 1.63×10^{19} Cu atom m^{-2}. Prior to the measurement, 150 mg of sample was reduced at 350 °C for 0.3 h in N_2/H_2 (30/5 ml min^{-1}) mixed gas flow.

N_2 adsorption (−196 °C) study was used to obtain the BET surface area of the mixed oxides. The measurement was carried out on a Micromeritics Flow Sorb II2300 instrument. The samples after the calcination were pretreated in vacuum at 300 °C for 30 min before the measurements.

2.3. Catalytic reactions and analyzes of the products

The water–gas shift reaction was carried out using a fixed bed reactor at atmospheric pressure. A U-shaped Pyrex glass tube with inner diameter of 4 mm was used as a reactor. Typically 200 mg of catalyst, which has been pelletized and sieved to 0.25–0.42 mm in diameter, was loaded into the reactor together with 200 mg of quartz beads. The catalyst was treated in a mixed gas flow of N_2/H_2 (30/5 ml min^{-1}) at 350 °C for 20 min and then purged with He (purity, 99.99%). The reaction was started by introducing a gas mixture of 1.45% CO in water and nitrogen to the reactor. Typically mixed gas flow of $CO/H_2O/N_2$ (0.7/2.2/47.1 ml-NTP min^{-1}) was supplied for the reaction, where N_2 was used as the internal standard for the calculations of the conversions of CO and H_2O. H_2O was fed by bubbling a mixed gas of CO and N_2 into water in the reservoir which was controlled at the desired temperature. In the present work, CO_2 was not included in the reactant gas although the shift reaction in the actual reformer is the equilibration of reformate mixture. Such conditions were selected to see more precisely kinetically controlled reactions under the low CO conversion (vide infra).

The products were analyzed by on-line gas chromatographs (GC). A GC with packed molecular sieves 5 A column (3 m, φ 1/4), He carrier gas and TCD were used to analyze N_2 and CO. Another GC with packed molecular sieves 5 A column (3 m, φ 1/4), Ar carrier gas and TCD were used to analyze H_2, N_2 and CO. CO_2 and H_2O were also quantified by another GC with TCD using a packed PEG 20 M column (1 m, φ 1/4). All the lines and valves through the water feed, the reactor, the exit and the gas chromatographs were heated to 130 °C to prevent the condensation of water.

3. Results and discussion

3.1. Structure of hp-Cu/MgO/ZnO catalysts

Fig. 1 shows the XRD patterns of hp-Cu/ZnO (45/55) (a) and hp-Cu/MgO/ZnO (45/10/45) (b) catalysts, after drying at 80 °C in air (-1), after the calcination at 300 °C for 3 h in air (-2) and after the shift reaction for 50 h (-3). The Mg content was increased from 0 to 10% at a constant Cu content of 45% in the raw materials for the catalyst preparation. XRD patterns of all catalysts showed the lines of aurichalcite $(Cu,Zn)_5(CO_3)_2(OH)_{16}$ after drying (a-1 and b-1), CuO and ZnO after calcination (a-2 and b-2), and Cu metal and ZnO after reaction (a-3 and b-3), independently on the apparent Mg content. No reflection line assigned to Mg species, MgO and $MgCO_3$, was observed. This is probably due to a very low content of MgO since Mg was not sufficiently incorporated in the catalyst during the hp-preparation (vide infra). No other species, such as malachite, $Cu_2(CO_3)(OH)_2$, and $Zn_4CO_3(OH)_6{\cdot}H_2O$, was observed in the hp-Cu/MgO/ZnO catalysts. After the calcination at 300 °C for 3 h, broad lines of CuO and ZnO appeared for all the hp-Cu/MgO/ZnO catalysts (a-2 and b-2). After the shift reaction at 250 °C for 50 h, the lines of Cu metal and ZnO were observed; the former were strengthened in the Mg rich compositions (b-3), whereas the latter were sharpened in the Zn rich compositions (a-3).

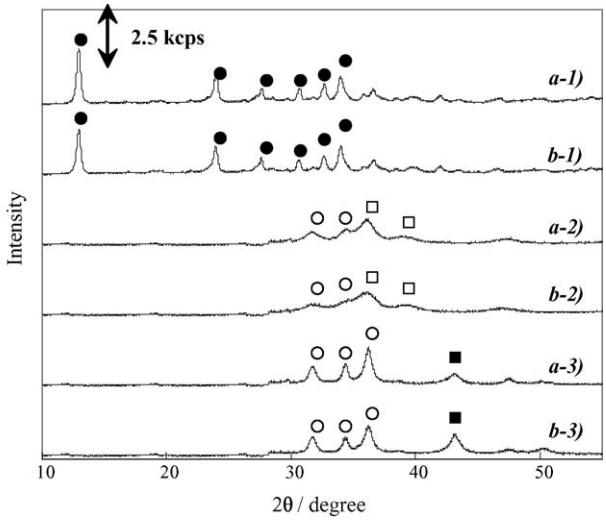

Fig. 1. XRD patterns of hp-Cu/MgO/ZnO catalyst. (a-1) hp-Cu/ZnO (45/55) after drying in air at 80 °C; (b-1) hp-Cu/MgO/ZnO (45/10/45) after drying in air at 80 °C; (a-2) hp-Cu/ZnO (45/55) after calcination at 300 °C for 3 h; (b-2) hp-Cu/MgO/ZnO (45/10/45) after calcination at 300 °C for 3 h; (a-3) hp-Cu/ZnO (45/55) after reaction for 50 h; (b-3) hp-Cu/MgO/ZnO (45/10/45) after reaction for 50 h. (●) Aurichalcite $(Cu,Zn)_5(CO_3)_2(OH)_{16}$; (◯) ZnO; (□) CuO; (■) Cu metal.

Cu K-edge XANES spectra of the hp-Cu/MgO/ZnO catalyst after the calcination and reference compounds are shown in Fig. 2(A). Cu foil shows an edge at 8979 eV and two characteristic peaks at the higher energy (Fig. 2(A)(a)). Cu_2O and CuO possess different coordination and electronic structures, showing quite different spectra: the latter oxide possesses a distorted octahedral coordination centered at Cu^{2+} and shows an edge at 8984 eV (Fig. 2(A)(c)). All catalyst samples, i.e. hp-Cu/ZnO (50/50), hp-Cu/MgO/ZnO (45/2/53) and hp-Cu/MgO/ZnO (45/15/40), show spectra quite similar to that of CuO, suggesting that Cu species basically exists as CuO in the catalysts. However, the edges at 8984 eV of both hp-Cu/MgO/ZnO (45/2/53) and hp-Cu/MgO/ZnO (45/15/40) are weaker than those of hp-CuO/ZnO and CuO. Moreover, the edges of hp-Cu/MgO/ZnO (45/2/53) and hp-Cu/MgO/ZnO (45/15/40) shifted toward the lower energy side compared to

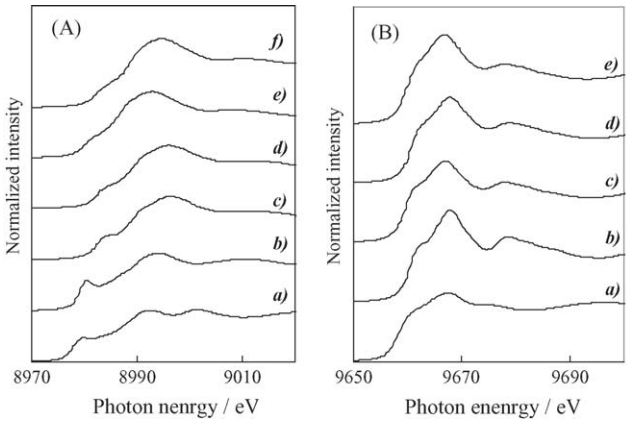

Fig. 2. Cu (A) and Zn (B) K-edge XANES spectra of hp-Cu/MgO/ZnO catalyst and reference compounds. (A): (a) Cu foil; (b) Cu_2O; (c) CuO; (d) hp-Cu/ZnO (50/50); (e) hp-Cu//MgOZnO (45/2/53); (f) hp-Cu/MgO/ZnO (45/15/40); (B): (a) Zn foil; (b) ZnO; (c) hp-Cu/ZnO (50/50); (d) hp-Cu/MgO/ZnO (45/2/53); (e) hp-Cu/MgO/ZnO (45/15/40).

those of hp-CuO/ZnO and CuO. These results indicate that the distortion of octahedron around Cu^{2+} is smaller, whereas electron density on Cu^{2+} is larger, in the Mg-containing catalysts than in hp-CuO/ZnO and CuO. Zn K-edge XANES spectra of the hp-Cu/MgO/ZnO catalyst after the calcination and reference compounds are shown in Fig. 2(B). ZnO shows an edge at 9661 eV and two peaks at 9669 and 9680 eV (Fig. 2(B)(a)). No significant change was observed in the spectra at the lower energy between the catalyst samples and ZnO.

Fourier transforms of k^3-weighted Cu K-egde EXAFS spectra of the hp-Cu/MgO/ZnO catalysts after the calcination and reference compounds are shown in Fig. 3(A). The spectra were almost similar for all catalyst samples (Fig. 3(A)(d–f)), hp-CuO/ZnO, hp-Cu/MgO/ZnO (45/2/53) and hp-Cu/MgO/ZnO (45/15/40) showed peaks at 1.5 and 2.5 Å (non-phase-shift corrected), coinciding with the bond distance of Cu–O and Cu–Cu in CuO independently on the Mg content. Zn K-egde EXAFS spectra (Fig. 3(B)) were also similar for all catalyst samples, hp-CuO/ZnO, hp-Cu/MgO/ZnO (45/2/53) and hp-Cu/MgO/ZnO (45/15/40), and showed peaks of ZnO independently on the Mg content. These indicate that both Cu and Zn species exist as CuO and ZnO in the catalyst. In the Cu-EXAFS spectra (data not shown), the phases of the EXAFS oscillation for all catalyst samples were quite similar, whereas the amplitude for hp-catalyst were weaker than that for cp-catalyst. This indicates that the particle size of CuO is smaller in the hp-catalyst than in the cp-catalyst, coinciding with the results observed by XRD analyzes in the previous paper [26].

Table 1
Effect of the addition of alkaline-earth metal oxides on hp-Cu/ZnO catalysts

Catalyst[a]	BET surface area ($m^2\ g_{cat}^{-1}$)	Cu^0 surface area ($m^2\ g_{cat}^{-1}$)	CO conversion (%)[b]
hp-Cu/ZnO (45/55)	81.8	37.3	89.7
hp-Cu/MgO/ZnO (45/2/53)	74.7	40.1	93.4
hp-Cu/CaO/ZnO (45/2/53)	72.2	37.9	90.5
hp-Cu/SrO/ZnO (45/2/53)	75.8	47.0	84.9
hp-Cu/BaO/ZnO (45/2/53)	71.6	33.2	90.6

[a] Number in the parenthesis shows the ratio of Cu/Me/Zn (Me: alkaline-earth metal) in the raw materials for the catalyst preparation.
[b] Reaction temperature: 150 °C.

3.2. Activity of hp-Cu/MgO/ZnO catalysts

The effects of the addition of alkaline-earth metal oxides on the catalytic activity of hp-Cu/ZnO are shown as CO conversion together with the BET surface area and Cu-metal surface area in Table 1. The correct evaluation of the effects of these additions is difficult since the amounts of the alkaline-earth metals in these catalysts were not quantitated (vide infra); MgO afforded the highest CO conversion among the alkaline-earth metal oxides tested. Cu metal surface area increased even though the BET surface area decreased by the addition of MgO. The addition of CaO and BaO showed no substantial effect on the activity; both

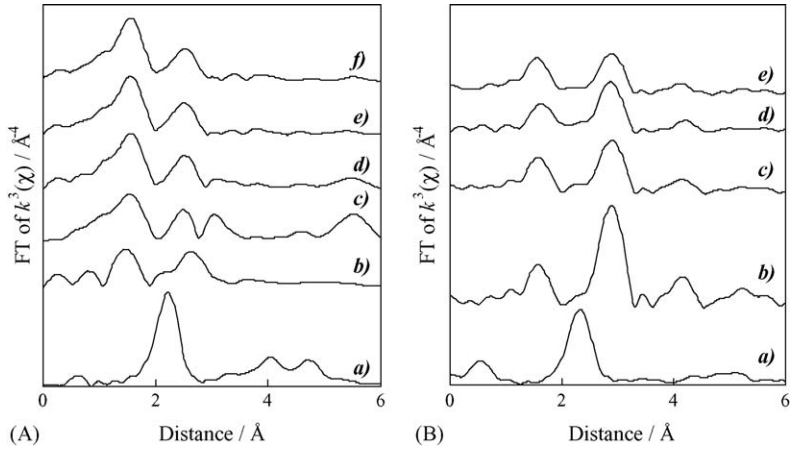

Fig. 3. Fourier transforms of k^3-weighted Cu (A) and Zn (B) K-egde EXAFS spectra of hp-Cu/MgO/ZnO catalyst and reference compounds. (A): (a) Cu foil; (b) Cu_2O; (c) CuO; (d) hp-Cu/ZnO (50/50); (e) hp-Cu//MgO/ZnO (45/2/53); (f) hp-Cu/MgO/ZnO (45/15/40); (B): (a) Zn foil; (b) ZnO; (c) hp-Cu/ZnO (50/50); (d) hp-Cu/MgO/ZnO (45/2/53); (e) hp-Cu/MgO/ZnO (45/15/40).

Table 2
Effect of the preparation method on the activity of the Cu catalysts

Catalyst[a]	BET surface area ($m^2\ g_{cat}^{-1}$)	Cu^0 surface area ($m^2\ g_{cat}^{-1}$)	CO conversion (%)[b]
hp-Cu/ZnO (45/55)	81.8	37.3	89.7
cp-Cu/ZnO (45/55)	84.3	30.1	70.7
hp-Cu/MgO/ZnO (45/2/53)	74.7	40.1	93.4
cp-Cu/MgO/ZnO (45/2/53)	81.1	32.7	72.1

[a] Number in the parenthesis shows the ratio of metals in the raw materials for the catalyst preparation.
[b] Reaction temperature: 150 °C.

metal oxides brought rather decline on both the BET surface area and Cu metal surface area. Although both the BET surface area and Cu metal surface area were the highest, the activity of hp-Cu/SrO/ZnO was the lowest among the catalysts tested. Effect of the preparation method of binary Cu/ZnO and ternary Cu/MgO/ZnO catalysts is shown in Table 2. The hp-method afforded larger Cu metal surface area, resulting in the higher activity, than the cp-method, although the BET surface area was larger for cp-catalysts than for hp-catalysts.

The effects of the Mg content on the activity of the hp-Cu/MgO/ZnO catalysts for the shift reaction are shown in Fig. 4, together with the BET surface area and Cu metal surface area. Mg/(Cu + Mg + Zn) at.% were obtained by ICP analyzes. The values obtained were far smaller than those in the raw materials, indicating that Mg could not be efficiently incorporated in the catalyst. This is probably due to pH value at 7.0 in the catalyst preparation, since Mg easily dissolved in acidic or neutral aqueous solution. It was reported that the isoelectric point (pH_{IEP}) of brucite ($Mg(OH)_2$) was close to 11 and that steady-state dissolution rates of brucite were high in neutral to acid solution ($pH \leq 8$), whereas the rates decreased abruptly in alkaline solution ($pH > 8$) [32]. Addition of 0.1 at.% of Mg caused a significant increase in the CO conversion as well as in the Cu metal surface area (Fig. 4). The BET surface area showed

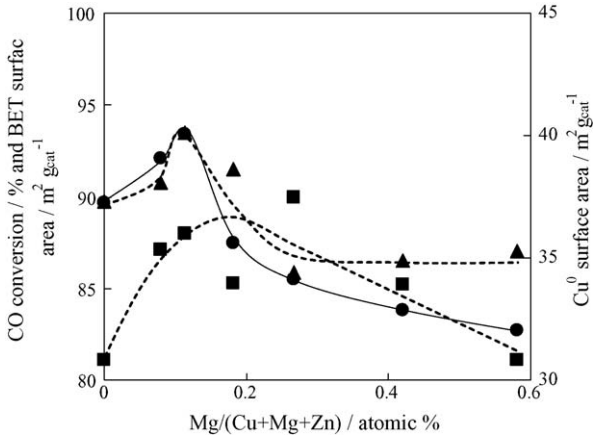

Fig. 4. Activity and physical properties of hp-Cu/MgO/ZnO catalyst. Catalyst, 200 mg; flow rate: $CO/H_2O/N_2 = 0.7/2.2/47.1$ ml-NTP min^{-1}; reaction temperature, 150 °C. (–●–) CO conversion; (···▲···) Cu^0 surface area; (···■···) BET surface area.

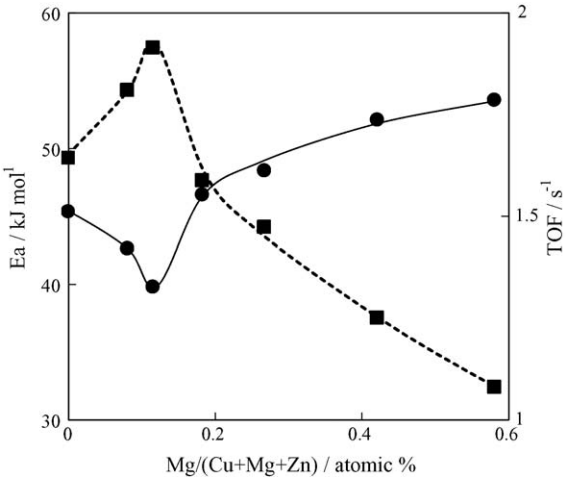

Fig. 5. Activation energy and turnover frequency of hp-Cu/MgO/ZnO catalyst. (–●–) Activation energy; (···■···) turnover frequency. Catalyst, 200 mg; flow rate: $CO/H_2O/N_2 = 0.7/2.2/47.1$ ml-NTP min^{-1}; reaction temperature, 100–200 °C for E_a and 110 °C for TOF.

also the maximum value at 0.11 at.% in the Mg content, but the dependency of the CO conversion was more obvious on the Cu metal surface area than on the BET surface area.

Apparent activation energies (E_a) and turnover frequencies (TOFs) were calculated from the rates of CO consumption over the hp-Cu/MgO/ZnO catalysts between 100 and 200 °C and at 110 °C, respectively (Fig. 5). These conditions are far from thermodynamic equilibrium and were chosen to see more precisely kinetically controlled reaction in the absence of CO_2. TOFs were calculated based on copper metal surface area assuming two Cu atoms per oxygen atom and a Cu surface density of 1.63×10^{19} Cu atom m^{-2} in N_2O decomposition. The values of E_a and TOFs showed the minimum and the maximum values, respectively, at the Mg content of 0.11 at.%, indicating that the nature of the active site was modified by the addition of small amount of Mg. Oxidation state of Cu species on the hp-Cu/MgO/ZnO catalysts pre-reduced at 300 °C for 1 h was studied by AES and XPS measurements. Auger electron spectra of Cu species on hp-catalysts are shown in Fig. 6. According to the data reported by Batista et al. [33], Cu^0 and Cu^+ species have the kinetic energies (Cu-LMM) of 918.6 and 916.5 eV, respectively. A peak assigned to Cu^+ was intensively observed at 916.3 eV together with a weak peak of Cu^0 at 918.3 eV in the Cu-LMM Auger spectrum of hp-Cu/MgO/ZnO (45/2/53) (Fig. 6(b)). The hp-Cu/ZnO (45/55) sample also showed both peaks of Cu^+ and Cu^0, while the former intensity was not so high (Fig. 6(a)). Moreover a satellite peak characteristic of Cu^{2+} was unobservable around 945 eV in the XPS of Cu $2p_{3/2}$ on hp-Cu/MgO/ZnO (45/2/53) (data not shown) [34]; thus, the oxidation state of Cu could be zero- or mono-valent. It is therefore concluded that the formation of Cu^+ species was enhanced by the addition of Mg to hp-Cu/ZnO.

3.3. Active sites on hp-Cu/MgO/ZnO catalysts

STEM-EDS images of the hp-Cu/MgO/ZnO (45/2/53) catalysts after the shift reaction are shown in Fig. 7, in which white

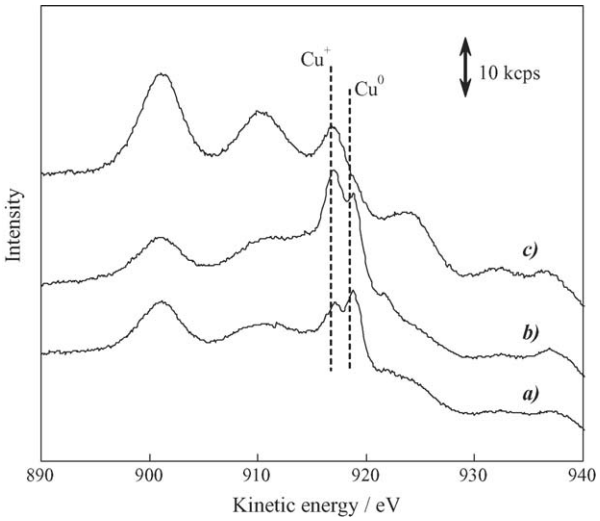

Fig. 6. Auger electron spectra of hp-Cu/ZnO (45/55) (a), hp-Cu/MgO/ZnO (45/2/53) (b) and hp-Cu/ZnO (45/55) treated by steam (c). (c) hp-Cu/ZnO (45/55) pre-reduced in a mixed gas flow of N_2/H_2 (30/5 ml min^{-1}) at 350 °C for 20 min was treated in a mixed gas flow of N_2/H_2O (45/2 ml min^{-1}) at 150 °C for 60 min.

spots show the presence of each metal species. It is clearly seen that Cu metal and ZnO are quite separately distributed, while Mg is rather uniformly distributed on both Cu metal and ZnO. The calculated results from the line width in XRD (vide infra) showed that the average sizes of Cu metal particles on the catalysts are less than 15 nm, whereas those of ZnO are 30–40 nm in all the catalyst samples tested. The Mg content was less than 1 at.% and any reflection lines of MgO was not observed in the XRD. Therefore, it is likely that small-sized Cu metal particles located on large-sized ZnO crystals and MgO distributed on or in both Cu metal and ZnO particles.

Apparent activation energy (E_a) was plotted against Cu metal particle size for the catalyst samples, hp-Cu/ZnO (45/55) and hp-Cu/MgO/ZnO (45/2/53), which were pre-reduced under varying conditions (Fig. 8). Before the shift reaction, the catalyst was treated in a mixed gas flow of N_2/H_2 (30/5 ml min^{-1}) at varying temperature and for varying time as shown in parentheses in Fig. 8. For each catalyst, a good correlation was observed between E_a and Cu metal particle size, indicating that E_a decreased with decreasing Cu metal particle size. This is probably due to an increase in the surface area of Cu metal, i.e. increase in the active site, with decreasing Cu metal particle size. Moreover, hp-Cu/MgO/ZnO (45/2/53) clearly showed the lower values of E_a compared with those of hp-Cu/ZnO (45/55), sug-

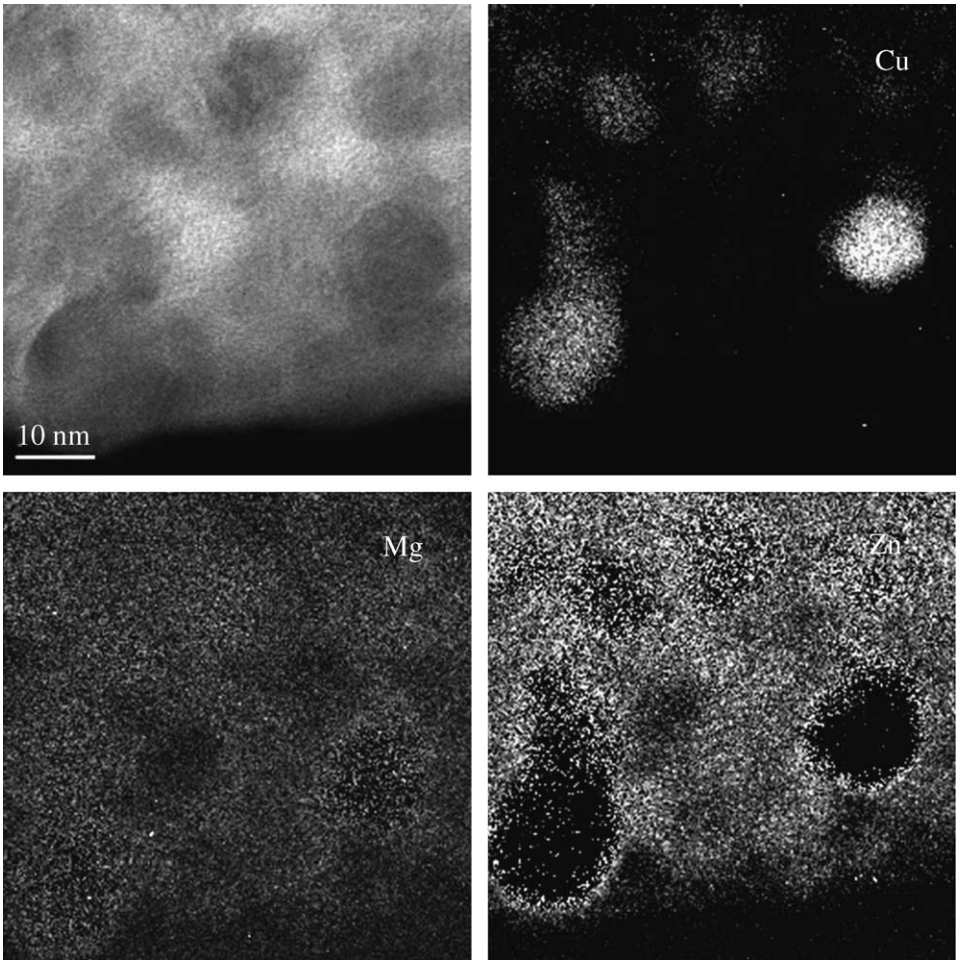

Fig. 7. STEM-EDS images of hp-Cu/MgO/ZnO (45/2/53) catalysts.

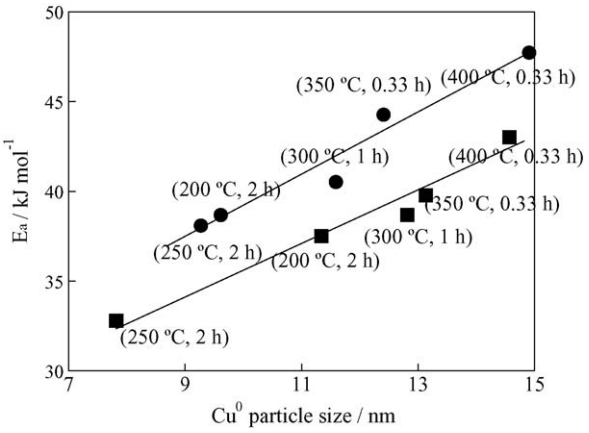

Fig. 8. Activation energy and Cu metal particle size of hp-Cu/ZnO (45/55) and hp-Cu/MgO/ZnO (45/2/53) catalysts reduced under various conditions. (●) hp-Cu/ZnO (45/55); (■) hp-Cu/MgO/ZnO (45/2/53). All samples were pre-reduced in a mixed gas flow of N_2/H_2 (30/5 ml min^{-1}) and used in the shift reaction.

gesting that the nature of active site is different from each other over the two catalysts. E_a was in the range of 30–50 kJ mol^{-1}, which are rather low values compared with those reported for Cu (1 1 1) (71.1 kJ mol^{-1}) [35], Cu/Al_2O_3 (59.3 kJ mol^{-1}) and $Cu/ZnO/Al_2O_3$ (78.2–86.5 kJ mol^{-1}) [36], Cu/MnO_2 (55.0 kJ mol^{-1}) [37] and $Cu/ZnO/Cr_2O_3$ (112 kJ mol^{-1}) [38].

Two plausible mechanisms have been proposed in the shift reaction over Cu catalysts: one is the formate intermediate mechanism [36,39] and another is the surface reduction–oxidation mechanism [40–44]. It was found to be important especially at high pressure to include in the mechanism the synthesis and hydrogenation of formate intermediate [36]. In the formate intermediate mechanism, H_2O dissociates to $OH_{(a)}$ and then $OH_{(a)}$ reacts with CO to form a formate intermediate which finally decomposes to CO_2. In the reduction–oxidation mechanism, the surface is oxidized by H_2O and subsequently reduced by CO to form CO_2. In both cases, H_2O dissociates, whereas CO is oxidized, on the catalyst surface. Frequently the O–H bond cleavage [41,43,44] and scarcely the CO oxidation [41,43] work as the rate-determining step of the shift reaction on Cu metal surface. In situ observation of Cu LMM Auger electron spectra of hp-Cu/ZnO (45/55) during the steam treatment is shown in Fig. 6(c); hp-Cu/ZnO (45/55) pre-reduced was treated in a mixed gas flow of N_2/H_2O (45/2 ml-NTP min^{-1}) at 150 °C for 60 min. A peak at 918.3 eV assigned to Cu^0 disappeared, whereas a peak at 915.4 eV assigned to Cu^+ was strengthened; the kinetic energy was slightly lower than the value 916.5 eV reported by Batista et al. [33]. This clearly indicates an occurrence of the oxidation of Cu^0 to Cu^+ during the steam treatment, suggesting that the shift reaction proceeds via the reduction–oxidation mechanism expressed by Eqs. (2) and (3):

$$2Cu + H_2O \rightarrow Cu_2O + H_2 \quad (2)$$

$$Cu_2O + CO \rightarrow 2Cu + CO_2 \quad (3)$$

It is most likely that Cu^+ sites observed on hp-Cu/MgO/ZnO are the active sites and locate at the surface boundary between Cu metal particles and ZnO crystals, where MgO assists their formations by stabilizing the cationic species. The cationic Cu^+ sites chemisorb CO as the first step of the reaction, followed by the reduction to Cu^0, which in turn provoke H_2O dissociation as well as O–H bond cleavage, resulting in an acceleration of the surface oxidation–reduction reactions (2) and (3).

According to the results of Auger electron spectra of the hp-Cu/ZnO and hp-Cu/MgO/ZnO catalysts after the reduction, peaks of both Cu^0 and Cu^+ species have been clearly observed (Fig. 6(a) and (b)). It is therefore concluded that Cu^+ species was formed on both hp-Cu/ZnO and hp-Cu/MgO/ZnO after the reduction and possibly worked as the active site for the shift reaction. When TOF values were calculated based on the Cu metal surface area, i.e. assuming two Cu atoms per oxygen atom and a Cu surface density of 1.63×10^{19} Cu atom m^{-2} in N_2O decomposition (dotted line in Fig. 5), the values increased with increasing Mg content up to 0.11 at.% and then decreased on hp-Cu/MgO/ZnO catalysts. This well agreed with the clear dependency of activation energy on the Mg content (solid line in Fig. 5), suggesting that the nature of the Cu active site varies depending on the Mg content on the hp-Cu/MgO/ZnO catalysts. It is likely that the shift reaction was catalyzed via a reduction–oxidation mechanism between Cu^0 and Cu^+, in which Cu^+ sites chemisorbed and oxidized CO to CO_2 to form Cu^0, whereas the reduced Cu^0 sites were reoxidized by H_2O to form Cu^+ and H_2 (Figs. 6(c)) [42,43]. However, a close similarity was still observed in the activity pattern and the exposed Cu metal surface area determined by N_2O adsorption/decomposition test (dotted line in Fig. 4). In spite of the hypothesis of Cu^+ active sites, an important role Cu^0 cannot be totally denied since the reaction proceeded by the reduction–oxidation mechanism between Cu^0 and Cu^+. Moreover, the amount of Cu^+ sites reasonably depends on the particle size of Cu metal if Cu^+ forms at the boundary between Cu metal particles and ZnO particles, suggesting an apparent dependency of the activity on Cu^0 species. As a result, the amount of Cu^+ sites increased with decreasing Cu metal particle size, resulting in an increase in the activity as observed in a decrease in E_a (Fig. 8).

3.4. Stability of hp-Cu/MgO/ZnO catalysts

It is well known that the commercial Cu catalysts are very sensitive against the reduction treatments and the reduction under severe conditions frequently resulted in the deactivation of the catalysts. This can be well explained by the sintering of Cu metal particles. Time courses of the shift reactions over hp-Cu/MgO/ZnO (45/2/53), hp-Cu/ZnO (45/55) and a commercial $Cu/ZnO/Al_2O_3$ catalyst are shown in Fig. 9. The commercial catalyst showed more stable activity when pre-reduced at 200 °C than at 250 °C, showing that the reduction treatment at high temperature frequently caused a sintering of Cu metal over the catalysts resulting in the deactivation. Interestingly, both hp-Cu/ZnO (45/55) and hp-Cu/MgO/ZnO (45/2/53) showed higher stability when pre-reduced at 250 °C than at 200 °C, suggesting that hp-preparation provide the Cu catalysts with the high stability. Especially the hp-Cu/MgO/ZnO catalyst showed a high and stable activity for 50 h in the shift reaction when pre-reduced at 250 °C. It must also be pointed out that the reduction of hp-

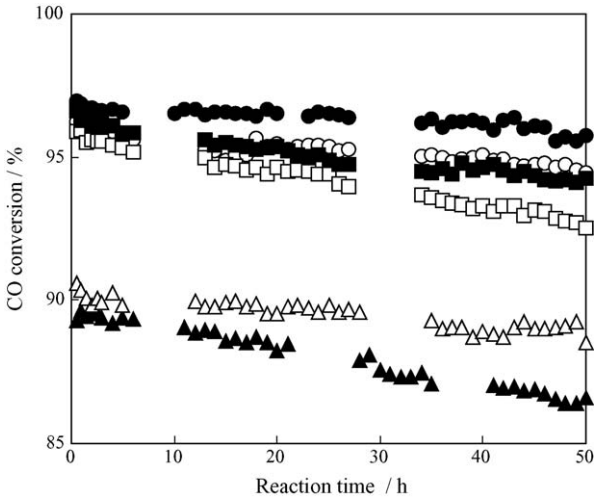

Fig. 9. Sustainability of hp-Cu/MgO/ZnO (45/2/53) catalysts in the shift reaction. hp-Cu/MgO/ZnO (45/2/53): (●) reduced at 250 °C; (◯) reduced at 200 °C. hp-Cu/ZnO (45/55): (■) reduced at 250 °C; (□) reduced at 200 °C. Commercial $Cu/ZnO/Al_2O_3$: (▲) reduced at 250 °C; (△) reduced at 200 °C.

Cu/ZnO and hp-Cu/MgO/ZnO at 250 °C for 2 h resulted in the lower activation energies than those at 200 °C for 2 h (Fig. 8), which is exceptional from the view point of the effect of the reduction temperature on the activity of Cu catalysts. This activation energy of the hp-Cu/MgO/ZnO catalyst was the lowest among those obtained in a series of experiments. Both hp-Cu/ZnO and hp-Cu/MgO/ZnO showed the more stable activity by the reduction at the higher temperature of 250 °C, and the activities of these catalysts were higher than that of the commercial $Cu/ZnO/Al_2O_3$ catalyst (Fig. 9).

The stability of hp-catalysts was also supported by the measurements of Cu metal particle sizes after the shift reaction for 50 h (Table 3). During the shift reaction for 50 h, no significant increase in Cu metal particle size was observed over both hp-Cu/ZnO (45/55) and hp-Cu/MgO/ZnO (45/2/53) pre-reduced at 250 °C, whereas clear increases were observed when both catalysts were pre-reduced at 200 °C. In contrast, over the commercial Cu catalysts, pre-reduction at 200 °C was rather effective for keeping the Cu metal particle size than that at 250 °C (Table 3). SEM-EDS images clearly showed the homogeneous distribution of MgO in the hp-Cu/MgO/ZnO catalyst particles. It is likely that a small amount of MgO enhanced the formation or the stabilization of Cu^+ species on hp-Cu/ZnO catalyst. These results clearly indicate that hp-preparation can afford the sustainability on the Cu catalyst. This is probably due to the homogeneity of metal components in the catalyst prepared, which results in strong metal-support interactions on the catalyst. Usually Al_2O_3 was added as the third component in the commercial Cu/ZnO shift catalyst and it was reported that Al_2O_3 afforded high Cu dispersion as well as high catalyst stability. However, in the present shift reaction, Al_2O_3 was not effective as the third component although Al_2O_3 afforded actually high Cu dispersion as seen in the previous work [27]. Contrarily MgO was rather effective as the third component in the present work. This is an interesting point of this work and the effect of MgO will be clarified by a further investigation.

Table 3
Cu^0 particle size in the Cu catalysts before and after the reaction[a]

Catalyst[b]	Cu^0 particle size (nm)	
	Before	After
hp-Cu/ZnO (45/55)[c]	9.1	13.6
hp-Cu/MgO/ZnO (45/2/53)[c]	9.9	12.5
Commercial $Cu/ZnO/Al_2O_3$[c]	12.0	13.1
hp-Cu/ZnO (45/55)[d]	9.3	10.1
hp-Cu/MgO/ZnO (45/2/53)[d]	9.7	10.1
Commercial $Cu/ZnO/Al_2O_3$[d]	13.1	14.9

[a] Reaction time: 50 h.
[b] Number in the parenthesis shows the ratio of metals in the raw materials for the catalyst preparation.
[c] Pre-reduced at 200 °C.
[d] Pre-reduced at 250 °C.

4. Conclusions

Ternary Cu/MgO/ZnO catalysts were prepared by homogeneous precipitation (hp) using urea hydrolysis and successfully applied in the water–gas shift reaction. The catalyst precursors after the precipitation was composed of aurichalcite, $(Cu,Zn)_5(CO_3)_2(OH)_{16}$, which decomposed to a mixture of CuO and ZnO after the calcination. The amount of Mg actually included in the catalyst was less than 1.0 at.%. The highest and the most stable activity were obtained over the hp-Cu/MgO/ZnO catalysts due to a large Cu metal surface area as well as small Cu metal particle size. The addition of ∼0.1 at.% of Mg was the most effective, resulting in the highest activity as well as the lowest activation energy. Even after the pre-reduction at 250 °C, the hp-Cu/MgO/ZnO catalyst showed no significant decrease in the activity as well as no detectable sintering in the Cu metal particles during 50 h of the reaction, indicating that hp-Cu/MgO/ZnO is a promising candidate for the catalyst for the shift reaction. The formation of Cu^+ was observed on the hp-Cu/MgO/ZnO catalyst where the addition of MgO clearly enhanced the Cu^+ formation. In situ steam treatment of hp-Cu/ZnO resulted in the formation of the Cu^+ species on the catalyst surface. It was concluded that the Cu^+ active species were stabilized by MgO and catalyzed the shift reaction via the surface reduction–oxidation mechanism.

References

[1] F. Boccuzi, A. Chiorino, M. Manzoli, D. Andreeva, T. Tabakova, J. Catal. 188 (1999) 176.
[2] J.M. Zalc, V. Sokolovskii, D.G. Löffler, J. Catal. 206 (2002) 169.
[3] X. Wang, R.J. Gorte, J.P. Wagner, J. Catal. 212 (2002) 225.
[4] A. Luengnaruemitchai, S. Oosuwan, E. Gulari, Catal. Commun. 4 (2003) 215.
[5] V. Idakiev, T. Tabakova, Z.-Y. Yuan, B.-L. Su, Appl. Catal. A 270 (2004) 135.
[6] N. Hua, H. Wang, Y. Du, M. Shen, P. Yang, Catal. Commun. 6 (2005) 491.
[7] R.J. Gorte, S. Zhao, Catal. Today 104 (2005) 18.
[8] C.H. Kim, L.T. Thompson, J. Catal. 230 (2005) 66.
[9] P. Panagiotopoulou, D.I. Kondarides, J. Catal. 225 (2004) 327.

[10] M.J.L. Ginés, N. Amadeo, M. Laborde, C.R. Apesteguía, Appl. Catal. A 131 (1995) 283.
[11] K. Sekizawa, S.-I. Yano, K. Eguchi, H. Arai, Appl. Catal. A 169 (1998) 291.
[12] J. Wu, M. Saito, J. Catal. 195 (2000) 420.
[13] T. Utaka, K. Sekizawa, K. Eguchi, Appl. Catal. A 194/195 (2000) 21.
[14] Y. Tanaka, T. Utaka, R. Kikuchi, K. Sasaki, K. Eguchi, Appl. Catal. A 238 (2003) 11.
[15] T. Utaka, T. Takeguchi, R. Kikuchi, K. Eguchi, Appl. Catal. A 246 (2003) 117.
[16] Y. Tanaka, T. Utaka, R. Kikuchi, T. Takeguchi, K. Sasaki, K. Eguchi, J. Catal. 215 (2003) 271.
[17] Y. Tanaka, T. Utaka, R. Kikuchi, K. Sasaki, K. Eguchi, Appl. Catal. A 242 (2003) 287.
[18] Y. Tanaka, T. Takeguchi, R. Kikuchi, K. Eguchi, Appl. Catal. A 279 (2005) 59.
[19] M. Rønning, F. Huber, H. Meland, H. Venvik, D. Chen, A. Holmen, Catal. Today 100 (2005) 249.
[20] T. Hayakawa, H. Harihara, A.G. Andersen, A.P.E. York, K. Suzuki, H. Yasuda, K. Takehira, Angew. Chem. Int. Ed. Engl. 35 (1996) 192.
[21] K. Takehira, T. Shishido, M. Kondo, J. Catal. 207 (2002) 307.
[22] K. Takehira, T. Shishido, P. Wang, T. Kosaka, K. Takaki, Phys. Chem. Chem. Phys. 5 (2003) 3801.
[23] K. Takehira, T. Shishido, P. Wang, T. Kosaka, K. Takaki, J. Catal. 221 (2004) 43.
[24] K. Takehira, T. Kawabata, T. Shishido, K. Murakami, T. Ohoi, D. Shoro, M. Honda, K. Takaki, J. Catal. 231 (2005) 92.
[25] T. Shishido, Y. Yamamoto, H. Morioka, K. Takaki, K. Takehira, Appl. Catal. A 263 (2004) 249.
[26] T. Shishido, M. Yamamoto, D. Li, Y. Tian, H. Morioka, M. Honda, T. Sano, K. Takehira, Appl. Catal. A 303 (2006) 62.
[27] R.J. Candal, A.E. Regazzoni, M.A. Blesa, J. Mater. Chem. 2 (1992) 657.
[28] G.J. de, A.A. Soler-Illia, R.J. Candal, A.E. Regazzoni, M.A. Blesa, Chem. Mater. 9 (1997) 184.
[29] H. Morioka, H. Tagaya, K. Karasu, J. Kadokawa, K. Chiba, J. Solid State Chem. 117 (1995) 337.
[30] J.B. Van Zon, D.C. Koningsberger, H.F.J. Van Blik, D.E. Sayers, J. Phys. Chem. 82 (1985) 5742.
[31] J.W. Evans, M.S. Wainwright, A.J. Bridgewater, D.J. Young, Appl. Catal. 7 (1983) 75.
[32] O.S. Pokrovsky, J. Schott, Geochim. Cosmochim. Acta 68 (2004) 31.
[33] J. Batista, A. Pintar, D. Mandrino, M. Jenko, V. Martin, Appl. Catal. A 206 (2001) 113.
[34] Y. Tanaka, R. Kikuchi, T. Takeguchi, K. Eguchi, Appl. Catal. B 57 (2005) 211.
[35] C.T. Campbell, K.A. Daube, J. Catal. 104 (1987) 109.
[36] C.V. Ovesen, B.S. Clausen, B.S. Hammershøi, G. Steffensen, T. Askgaard, I. Chorkendorff, J.K. Nørskov, P.B. Rasmussen, P. Stolze, P. Taylor, J. Catal. 158 (1996) 170.
[37] G.J. Hutchings, R.G. Copperthwaite, F.M. Gottschalk, R. Hunter, J. Mellow, S.W. Orchard, T. Sangiorgio, J. Catal. 137 (1992) 408.
[38] E.M. Cherednik, N.M. Morozov, M.I. Temkin, Kinet. Katal. 10 (1969) 603.
[39] T. van Herwijnen, W.A. de Jong, J. Catal. 63 (1980) 83.
[40] S.-I. Fujita, M. Usui, N. Takezawa, J. Catal. 134 (1992) 220.
[41] C.V. Ovesen, P. Stolze, J.K. Nørskov, C.T. Campbell, J. Catal. 134 (1992) 445.
[42] Y. Li, Q. Fu, M. Flytzani-Stephanopoulos, Appl. Catal. B 27 (2000) 179.
[43] N.A. Koryabkina, A.A. Phatak, W.F. Ruettinger, R.J. Farrauto, F.H. Ribeiro, J. Catal. 217 (2003) 233.
[44] O. Jakdetchai, T. Nakajima, J. Mol. Struct. 619 (2002) 51.